

Pressure-induced large valence transitions in Yb-Cu binary intermetallic systems

Hitoshi Yamaoka ^{1,*}, Ayako Ohmura ^{2,†}, Naohito Tsujii ³, Hirofumi Ishii ⁴, Nozomu Hiraoka ⁴,
Hitoshi Sato ⁵ and Masahiro Sawada ⁵

¹*RIKEN SPring-8 Center, 1-1-1 Kouto, Mikazuki, Sayo, Hyogo 679-5148, Japan*

²*Faculty of Science, Niigata University, Niigata 950-2181, Japan*

³*Research Center for Materials Nanoarchitectonics, National Institute for Materials Science, 1-2-1 Sengen, Tsukuba, Ibaraki 305-0047, Japan*

⁴*National Synchrotron Radiation Research Center, Hsinchu 30076, Taiwan*

⁵*Hiroshima Synchrotron Radiation Center, Hiroshima University, Higashi-Hiroshima, Hiroshima 739-0046, Japan*



(Received 11 December 2023; revised 24 March 2024; accepted 25 March 2024; published 17 April 2024)

Electronic and crystal structures of YbCu, YbCu₂, and YbCu_{6,5} under pressure were studied by high-resolution x-ray absorption spectroscopy (XAS) and x-ray diffraction. We found pressure-induced large valence transitions on the order of 0.3 in these Yb compounds. YbCu exhibited a first-order transition with a sudden change in the Yb valence at 4 GPa, at which a structural transition was not accompanied. With further increasing pressure, YbCu shows a structural transition from the FeB-type to the cubic CsCl-type structure around 10 GPa, where the Yb valence increases only gradually. In YbCu₂, a structural transition was not observed up to 11.8 GPa, while the Yb valence shows a rapid increase around 4–7 GPa, indicating a significant change in the electronic structure. Anomalous reentrant valence transition to a lower valence state was found at low pressures of 3–4 GPa in YbCu_{6,5} without the structural phase transition. It is suggested that the anomaly in YbCu_{6,5} is possibly correlated to the electronic structure of the Cu *d* band. On the other hand, we found that these anomalous large changes in the Yb valences were linked to anomalies in crystal structures although there were no structural phase transitions. Complementary to the measurements of XAS at the Yb *L*₃ absorption edge, we also performed XAS at the Cu-*L*₃ absorption edge and measured the valence band spectra at ambient pressure.

DOI: [10.1103/PhysRevB.109.155147](https://doi.org/10.1103/PhysRevB.109.155147)

I. INTRODUCTION

In rare-earth compounds, some of the elements such as Yb, Eu, Sm, and Ce often show the valence instability between the two charge states [1–3]. The 4*f* electrons of these elements have a localized nature, while the electronic state of the 4*f* electrons in the compounds is the result of the hybridization of the 4*f* electrons with conduction (*c*) electrons (*c*–*f* hybridization) which is characterized by the Kondo temperature (*T*_K) [4]. The valence of the rare-earth elements of these compounds is a measure of the *c*–*f* hybridization and the Kondo temperature, which could be controlled by chemical substitution, temperature, and pressure.

In Yb compounds, the Yb³⁺ state is favored under pressure because of the smaller ion radius of Yb³⁺ ions compared to that of Yb²⁺ ions. Pressure increases the Yb valence with decreasing the *c*–*f* hybridization and induces the magnetically ordered state through a quantum critical point (QCP) with increasing the Yb valence [5]. This behavior has been described within the Doniach phase diagram and the Anderson model [6,7]. Interestingly, in Yb compounds a theory predicts that further increase of the pressure decreases the Yb valence and there may be a second QCP because of the increase of

the hybridization [8]. This pressure range was on the order of more than around 100 GPa and the electronic structures of Yb compounds have not been explored so far in this high-pressure range.

Recently, on the other hand, direct measurements of the Yb valence under pressures have revealed that some Yb compounds showed an anomalous decrease of the Yb valence with pressure at low pressures. In YbCu_{4,5} a first-order valence transition to the divalent Yb state was found around 0.6–2.7 GPa [9]. This valence transition was accompanied by the structural transition at the same pressure range. Furthermore, in the cubic YbCu₅-based compounds the Yb valence was found to decrease with pressure without structural phase transition at low pressures less than 10 GPa, indicating a pressure-induced crossover from a localized 4*f*¹³ state to the valence fluctuation regime, which was not expected for Yb systems with the conventional *c*–*f* hybridization [10]. A similar pressure-induced anomaly of the Yb valence has been also observed in YbInCu₄-based compounds [11]. Anomalies of the decrease of the Yb valence under pressure in these systems have been found to correspond to anomalies in the crystal structure.

In this paper, we performed a systematic study of the electronic and crystal structures of the Yb-Cu binary intermetallic systems, the compositions of YbCu, YbCu₂, YbCu_{4,5}, YbCu₅, and YbCu_{6,5} [12–21]. The purpose of the paper is to clarify the pressure dependences in the crystal and electronic

*Corresponding author: hitoshi_yamaoka@mineo.jp

†Corresponding author: ohmura@phys.sc.niigata-u.ac.jp

structures of these compounds which have not been explored yet. One of the physically interesting matters is whether the pressure-induced anomaly in the Yb valence is a general phenomenon or not. Thus, it is vital to explore Yb systems that show the pressure-induced valence decrease at low pressure, other than YbCu_{4.5}, cubic YbCu₅-based, and YbInCu₄-based compounds [9–11]. To measure the electronic structures of YbCu, YbCu₂, and YbCu_{6.5} under pressure, we employ high-resolution x-ray absorption spectroscopy with a partial fluorescence mode (PFY-XAS) at the Yb-*L*₃ absorption edge [22–24]. Pressure dependences of the crystal structures were also measured. We found large changes in the valence of the order of 0.3 under pressure in YbCu and YbCu₂.

Lawrence *et al.* systematically measured the temperature dependence of Yb valence while changing *X* for Yb*X*Cu₄ (*X* = Ag, Cd, In, Mg, Tl, Zn), and discussed how the slow crossover of Yb valence changed [25]. In Yb*X*Cu₄, the crystal structure did not change even if *X* was changed, but in YbCu_{*x*}, the crystal structure changed when the Cu composition was changed as described below, and thus we also systematically measured the pressure dependence of the crystal structures. In this paper, we found a common feature between anomalous changes in the Yb valences and anomalies in crystal structures.

Complementary to the measurements of the electronic structure of the Yb site under pressure, we performed x-ray absorption spectroscopy at the Cu-*L*₃ absorption edge to measure that of the Cu site at ambient pressure. Additionally, the valence band spectra were measured at ambient pressure (see Supplemental Material [26]).

II. EXPERIMENTS

Polycrystalline samples of YbCu and YbCu₂ were prepared by melting the pure elements of Yb (99.9%) and Cu (99.99%) in a closed Nb tube. The Nb tubes were sealed by an arc furnace under argon atmosphere. Then, the tubes were sealed in evacuated quartz tubes and were heated in an electric furnace. For YbCu, the quartz tube was heated at 1223 K for 6 h and cooled to 873 K, at which the sample was annealed for 48 h. For YbCu₂, the quartz tube was heated at 1273 K for 1 h, and was homogenized at 1003 K for 12 h.

Polycrystalline samples of YbCu_{4.5} and YbCu_{6.5} were prepared by melting the elements in an arc furnace under argon atmosphere, and subsequently annealing. Slightly excess amounts of Yb were added to compensate for the loss of Yb during the arc melting. The melted ingots were wrapped with tantalum foils and were sealed in evacuated quartz tubes. Then the samples were annealed by heating the tubes at 1023 K for 2 weeks.

Homogeneities and chemical compositions of YbCu_{*x*} samples were confirmed by scanning electron microprobe and electron probe microanalysis. The backscattered electron images of the samples indicate that the samples were homogeneous and phase pure. The chemical compositions were almost in agreement with the stoichiometry of YbCu_{*x*}. The chemical composition observed for YbCu, YbCu₂, YbCu_{4.5} (Yb₂Cu₆), YbCu₅, and YbCu_{6.5} were Yb_{47.4}Cu_{52.6}, Yb_{31.1}Cu_{68.9}, Yb_{18.2}Cu_{81.8}, YbCu_{5.13}, and Yb_{14.8}Cu_{85.2}, respectively. In particular, the chemical composition for

YbCu_{4.5} was Yb 18.2% and Cu 81.8%, which is very close to that of YbCu_{4.5}. Therefore, the neighboring phases, such as YbCu_{4.4} and YbCu_{4.25}, are not relevant in the present experiment [27,28]. Crystal structure and physical parameters of YbCu, YbCu₂, YbCu_{3.5}, YbCu_{4.5}, and YbCu_{6.5} are summarized in Table I [9,12,15–21,29–35]. The effective magnetic moments of YbCu_{*x*} with higher Cu content at *x* ≥ 3.5 suggest nearly the Yb³⁺ valence state because the effective moment of a free Yb³⁺ ion is 4.54μ_B.

Measurements of the PFY-XAS spectra were performed at room temperature at the Taiwan beamline BL12XU, SPring-8 [36]. A Johann-type spectrometer equipped with a spherically bent Si(620) crystal (radius of ≈1 m) was used to analyze the Yb emission of 3*d*_{5/2} → 2*p*_{3/2} deexcitation following a 2*p*_{3/2} → 5*d* excitation with a solid state detector. The intensities of all sample spectra are normalized by the intensity of the incident beam monitor of an ion chamber just before the sample. The overall energy resolution was estimated to be about 1 eV around the emitted photon energy of 7400 eV from the elastic scattering. The high-pressure conditions were realized using a diamond anvil cell (DAC) with a Be gasket and the pressure-transmitting medium was silicone oil. The pressure was measured by the ruby fluorescence method [37,38]. A Be gasket 3 mm in diameter and approximately 100 μm thick was preindented to approximately 40–50 μm thick. The diameter of the sample chamber in the gasket was approximately 120 μm and the diamond anvil culet size was 300 μm. We used the Be gasket in-plane geometry where both incoming and outgoing x-ray beams passed through the Be gasket.

Pressure dependence of the x-ray diffraction (XRD) patterns was measured at BL12B2, SPring-8, using a CCD detection system at room temperature. For pressure generation, a three-pin plate diamond anvil cell (Plate DAC, Almax easyLab) was used with silicon oil as the pressure-transmitting medium. We take an arrangement of both incoming and outgoing x-ray beams passing through the diamonds with an incident photon energy of $h\nu = 18$ keV ($\lambda = 0.6888$ Å). A two-dimensional image of the CCD system was integrated by using the FIT2D program [39]. For YbCu₂ and YbCu_{6.5}, lattice constants and atomic positions were refined by the Rietveld method using the JANA2006 program [40–42]. Since the quality of the XRD patterns for YbCu was not good for the Rietveld method, we obtained its lattice constants analyzed by the Le Bail method also using the JANA2006 program. Examples of the fits are shown in the Supplemental Material [26]. Vacuum ultraviolet photoelectron spectroscopy (PES) was performed at the beam line BL-7, the Hiroshima Synchrotron Radiation Center (HiSOR), equipped with a hemispherical electron-energy analyzer (Gammadata-Scienta SES-2002). The energy resolution (ΔE) was set to approximately 150 meV at $h\nu = 182$ eV under vacuum pressure below 10⁻⁸ Pa. The Fermi edge of Au evaporated on the sample holder was used to calibrate the binding energy. Samples were fractured in vacuum just before the measurements. The energy resolution and the Fermi level are determined with a fit of the Fermi edge of Au using a convolution of Gaussian and Fermi-Dirac functions.

X-ray absorption spectra at the Cu-*L* absorption edge were measured at BL-14 at HiSOR with the total electron yield

TABLE I. Crystal structure and physical parameters of YbCu, YbCu₂, YbCu_{3.5}, YbCu_{4.5}, and YbCu_{6.5}. μ_{eff} , γ , and T_K are the effective magnetic moment, the specific heat coefficient, and the Kondo (or characteristic) temperature, respectively. The values of the Yb valence with an asterisk mark (*) are the values at ambient pressure estimated from the PFY-XAS spectra in this paper. YbCu_{6.5} is related to the CaCu₅ structure including the 18% Ca site occupied by pairs of Cu atoms [13]. YbCu_{4.5} is based on AuBe₅-type substructures with approximately 4570 and 2780 atoms per unit cell [27]. The crystal structure of YbCu_{4.5} was solved using x-ray diffraction and high-resolution transmission electron microscopy by Cerny *et al.* [20]: a monoclinically distorted $7 \times 7 \times 6.5$ superstructure of the cubic AuBe₅ structure type with 7448 atoms per unit cell.

	YbCu	YbCu ₂	YbCu _{3.5}	YbCu _{4.5}	YbCu ₅	YbCu _{6.5}
Crystal structure	Orthorhombic	Orthorhombic	Unknown		Cubic	Hexagonal
Type	FeB ^{a,b,c}	CeCu ₂ ^b		AuBe ₅ ^{c,d}	AuBe ₅ ^c	CaCu ₅ ^{c,e}
Yb valence	2.89 ^a , 2.37 ^f	2.39 ^f , 2.5 ^g	2.89 ^f , 2.7 ^b	2.96 ^f , 2.85 ^b , 2.95 ^h	2.97 ⁱ	2.40 ^f
Yb valence (present paper)	2.05*	2.20*				2.41*
μ_{eff} (μ_B)			4.12 ^j , 4.3 ^k	4.22 ^j , 4.36 ^f , 3.9 ^k	4.55 ^l	
γ (mJ/mol K ²)		6.8 ^m	90 ^b , 310 ^k	600 ⁿ , 635 ^o 740 ^q (0.82 GPa)	550 ^{l,p}	
T_K (K)				15 ^f	60 ^l	

^aRef. [17]; ^bRef. [18]; ^cRef. [19]; ^dRef. [20]; ^eRef. [13] f: Ref. [15]; ^gRef. [29]; ^hRef. [9]; ⁱRef. [30]; ^jRef. [12]; ^kRef. [31]; ^lRef. [16]; ^mRef. [32]; ⁿRef. [33]; ^oRef. [21]; ^pRef. [34]; ^qRef. [35].

mode, where the samples were fractured under the vacuum [43]. The energy resolution was set to be approximately less than 0.2 eV around 930 eV.

III. RESULTS AND DISCUSSION

A. XAS at the Yb- L_3 absorption edge

Pressure dependences of the PFY-XAS spectra of YbCu, YbCu₂, and YbCu_{6.5} are shown in Figs. 1(a)–1(c), respectively. In Fig. 1(d) we show an example of the fit of YbCu at 4.8 GPa assuming two Voigt functions for Yb²⁺, and those for Yb³⁺ with arctanlike backgrounds. The intensities of the two arctanlike backgrounds were determined to be proportional to the intensities of their corresponding Voigt functions of the Yb²⁺ and Yb³⁺ components. The mean valence is defined to be $v = 2 + I(3+)/[I(2+) + I(3+)]$, where $I(n+)$ is the intensity of the Ybⁿ⁺ component [44]. The Yb valences of YbCu, YbCu₂, and YbCu_{6.5} at ambient pressure were estimated to be 2.05, 2.20, and 2.41, respectively. In YbCu₂ earlier magnetic and lattice constant measurements suggested the Yb valence of 2.4–2.5 [45,46]. While the PES showed nearly the divalent Yb state of 2.18 later [47]. Present bulk-sensitive measurement supports the PES result.

Pressure dependence of the Yb valence of YbCu and YbCu₂ is shown in Figs. 1(e) and 1(f), respectively. In YbCu we found the first-order valence transition around 4 GPa, and the change in the Yb valence is reduced above 5 GPa. Similarly, in YbCu₂ a rapid change in the Yb valence was observed at pressure between 4 and 8 GPa, and further increase of the pressure does not change the Yb valence much above 8 GPa. Temperature-induced first-order valence transition of the Yb compounds has been observed in YbInCu₄ so far [44,48,49], but the first-order transition under pressure is rare.

In YbCu_{6.5} we found an anomalous pressure-induced change in the Yb valence. The Yb valence decreased rapidly in the pressure range between 3 and 4 GPa from 2.42 to 2.1 and increased gradually with further increase of the pressure as shown in Fig. 1(g). The magnetic Yb³⁺ state is favored commonly at high pressures in Yb compounds because of its

smaller ionic radius of the Yb³⁺ ion compared with that of the Yb²⁺ ion. The rare-earth metal theory predicted a return to the divalent state or the valence fluctuation region under the pressure with increasing the pressure up to a few hundred GPa (Mbar range) [8], which has not been observed experimentally so far, despite trials up to 202 GPa in Yb metal [50]. Therefore, the decrease of the Yb valence at low pressures in YbCu_{6.5} is highly anomalous, which cannot be understood by the conventional Anderson models. Recently, such pressure-induced anomalous valence crossover was found in YbCu_{4.5}, YbCu₅-based intermetallic compounds, and YbInCu₄-based compounds [9–11]. However, YbCu_{4.5} showed a possible structural transition around the pressure of the valence transition, while YbCu_{6.5} did not have a structural transition up to 17.4 GPa as shown below. The YbCu₅-based compounds also did not show any structural transition [10].

We also measured the temperature dependence of the PFY-XAS spectra of YbCu, YbCu₂, and YbCu_{6.5} (the results are not shown here). No temperature dependence of the Yb valence was observed within errors in these compounds.

B. XRD under pressure

Figures 2(a)–2(c) show the XRD patterns of YbCu, YbCu₂, and YbCu_{6.5} as a function of pressure, respectively. In YbCu the first-order valence transition occurred at 4 GPa as described above, but there is no structural transition up to 7.9 GPa. On the other hand, the XRD pattern of YbCu in Fig. 2(a) clearly demonstrates that a structural transition occurs at the pressure between 7.9 and 12.5 GPa. The high-pressure phase is most likely to be the cubic CsCl type as will be described below. Interestingly, the pressure-dependent Yb valence does not show a significant change in the pressure of the structural transition. In YbCu₂ the successive valence transition occurred around 4–7 GPa, while no structural phase transition was observed up to 11.8 GPa. In YbCu_{6.5} no structural transition was also observed up to 17.4 GPa as shown in Fig. 2(c). Thus, the first-order valence transition in YbCu, the successive valence transition in YbCu₂, and the anomalous

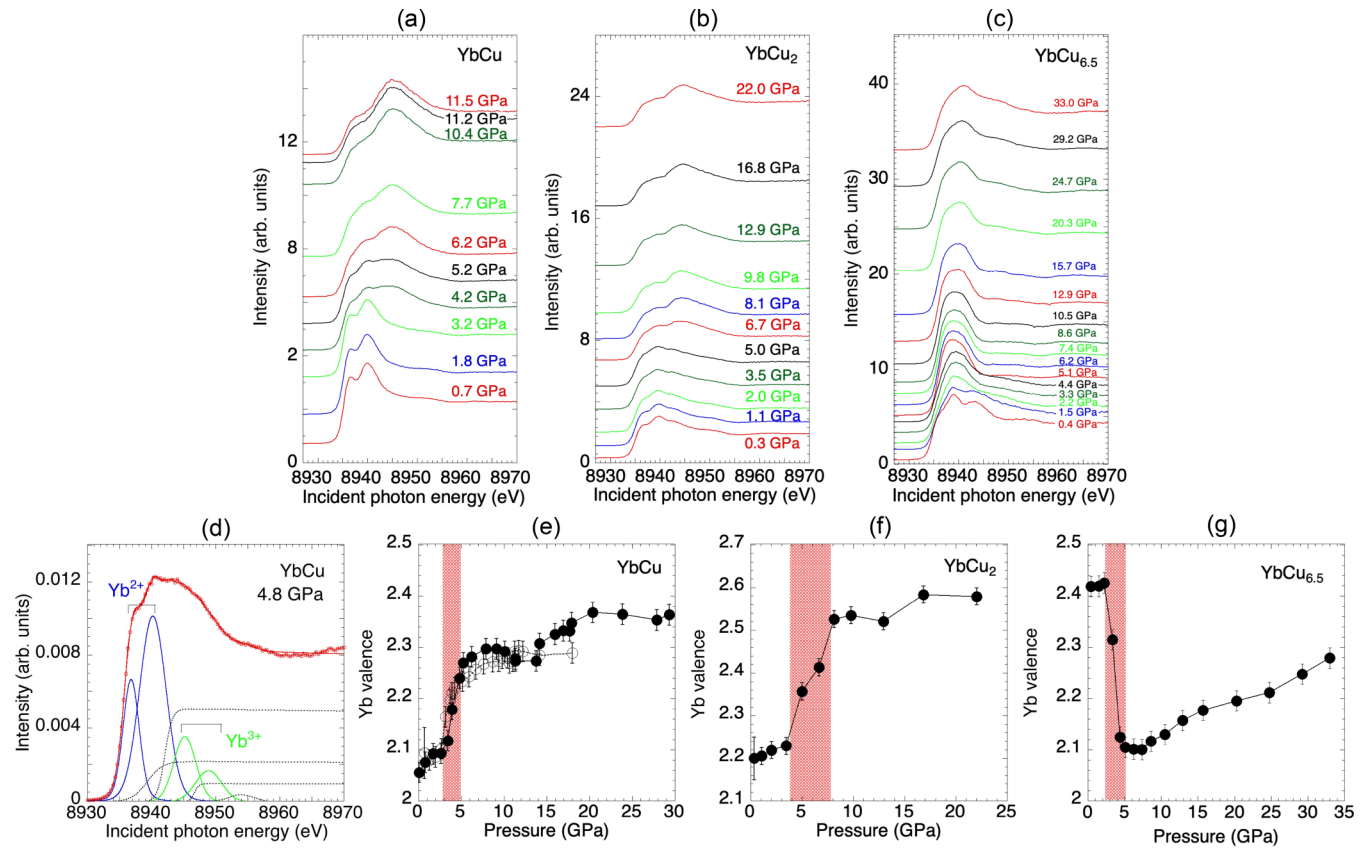


FIG. 1. (a)–(c) Pressure dependence of the PFY-XAS spectra for YbCu, YbCu₂, and YbCu_{6.5}, respectively. (d) A fit example of the PFY-XAS spectra of YbCu at 4.8 GPa. (e)–(g) Pressure dependence of the Yb valence of YbCu, YbCu₂, and YbCu_{6.5}, respectively. In panel (e) two independent measurements for YbCu are shown as closed and open circles. In panels (e)–(g) shaded areas correspond to the pressure range where the valence transitions occur.

decrease of the Yb valence at low pressure in YbCu_{6.5} do not accompany the structural phase transition.

Figure 3(a) shows a schematic view of the crystal structure of YbCu at lower pressures or at ambient pressure. Figures 3(b)–3(d) show the analyzed results of the XRD patterns in Fig. 2(a). The change in the volume was linear to pressure, and there was no particular anomaly as shown in

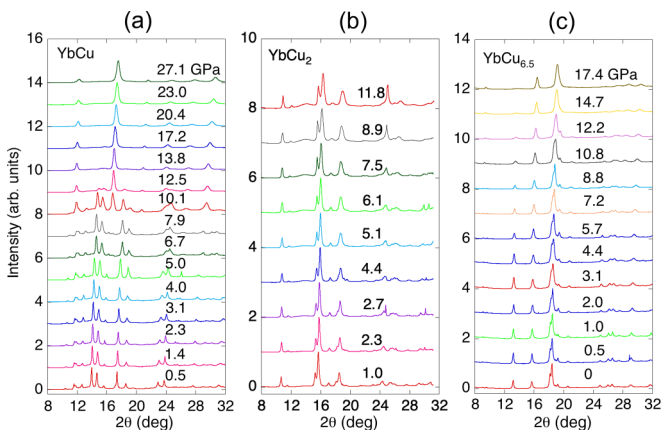


FIG. 2. (a)–(c) Pressure dependence of the XRD patterns for YbCu, YbCu₂, and YbCu_{6.5}, respectively.

In Fig. 3(b). In Fig. 3(c) it can be seen that compression along the *b* axis is less likely to occur than those along the *a* and *c* axes. This can be clearly seen in Fig. 3(d), which shows the ratios of the lattice constants. The XRD patterns of the high-pressure phase after the structural phase transition in YbCu could be fitted with the CsCl-type crystal structure as shown in Fig. 3(e). This is consistent with the crystal structures of *RCu* with *R* being the heavy rare-earth elements (Gd–Lu), for which the cubic CsCl type (*Pm-3m*) is reported to be stable [26,51–55]. The only exception is YbCu, where the crystal structure is reported to be the orthorhombic FeB type (*Pnma*) [18]. This is presumably attributed to the larger ionic size of Yb because of the nearly divalent state. Therefore, it is reasonable that the cubic CsCl-type YbCu is stabilized under high pressure. At high pressures above the structural phase transition, the volume and lattice constant decrease monotonically as shown in Figs. 3(f) and 3(g). In YbInCu₄ the first-order valence transition accompanied the structural phase transition [56]. On the other hand, in YbCu the structural phase transition starts to occur partially just above the pressure of the valence transition. This seems to suggest that the structural phase transition is triggered by the valence transition at the beginning of the structural transition, although the origin of the valence transition is not known.

Figure 4(a) shows a schematic view of the crystal structure of YbCu₂. Figures 4(b)–4(d) show the analyzed results of the XRD patterns in Fig. 2(b). The volume drops gradually in the

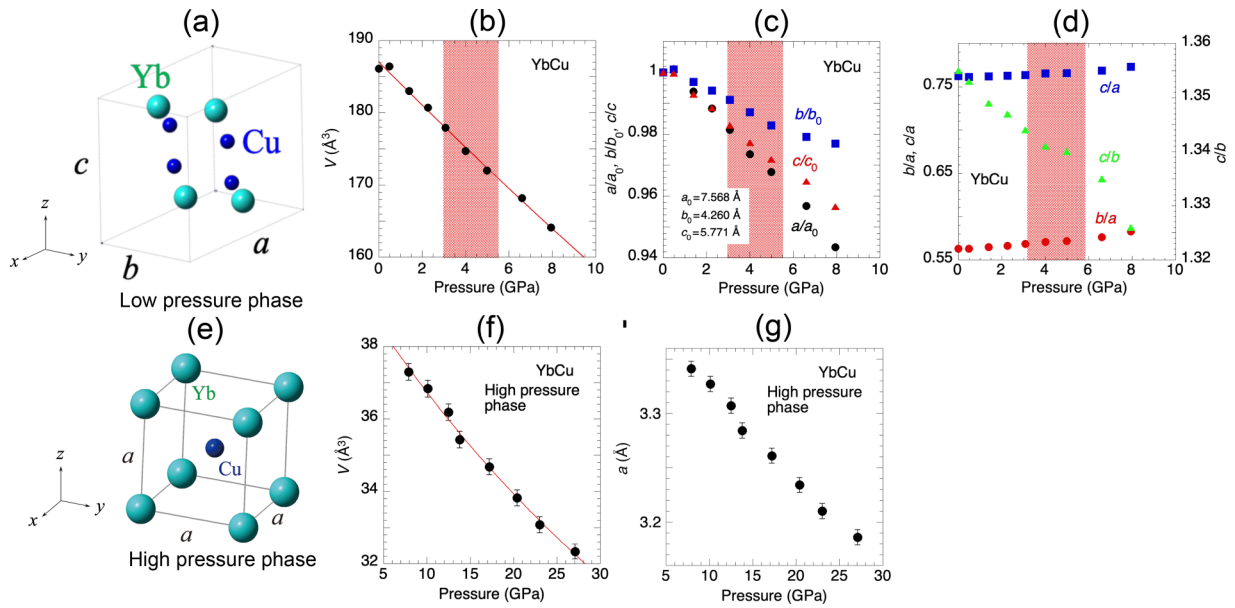


FIG. 3. (a) A schematic view of the YbCu crystal structure at low pressures before the structural phase transition. (b) Pressure dependence of the volume at a low-pressure phase. A shaded area corresponds to the pressure range of the valence transition in Fig. 1(e). (c) Pressure dependence of the normalized lattice parameters at a low-pressure phase. (d) Pressure dependence of the ratios of the lattice constants at a low-pressure phase. (e) Crystal structure at a high-pressure phase. (f) Pressure dependence of the volume at a high-pressure phase. (g) Pressure dependence of the lattice parameter at a high-pressure phase. For the data where the error is not visible, the error is less than or equal to the symbol size.

pressure range where the successive change in the Yb valence occurs as shown in Fig. 4(b). The lattice constant in Fig. 4(c) also changes in the same way as the volume changes. YbCu₂ is compressed more strongly along the *b* axis than along the *a* and *c* axes. This change can be clearly seen in the ratio between the axes in Fig. 4(d). The changes in the positions of Yb_z, Cu_y, and Cu_z are shown in Figs. S3(b) and S3(c) in the Supplemental Material [26]. Since the XRD peaks were broader in the high-pressure range and reliable results could not be obtained, the analyzed results of the atomic position and the atomic distance are shown only up to 9 GPa. The atomic position of Yb_z rises above about 7 GPa. The tendency of the change in the position of Cu in Fig. S3(c) is not clear.

Each atomic distance decreases with pressure as shown in Fig. S3(d), where pressure-induced changes are smaller or more stable at 6–9 GPa than the case less than 6 GPa. In the pressure region where the valence transition occurs, the change in the position of Cu becomes small, and Yb shifts along the *z* direction. No structural phase transitions have been observed in YbCu₂ in the pressure range measured, but these anomalous changes in volume and atomic position correlate to the valence transition.

Figure 5(a) shows a schematic view of the crystal structure of YbCu_{6.5}. Figures 5(b)–5(e) show the analyzed results of the XRD patterns in Fig. 2(c). Figures 5(b)–5(e) show volume, normalized lattice constants, a ratio of the lattice constants,

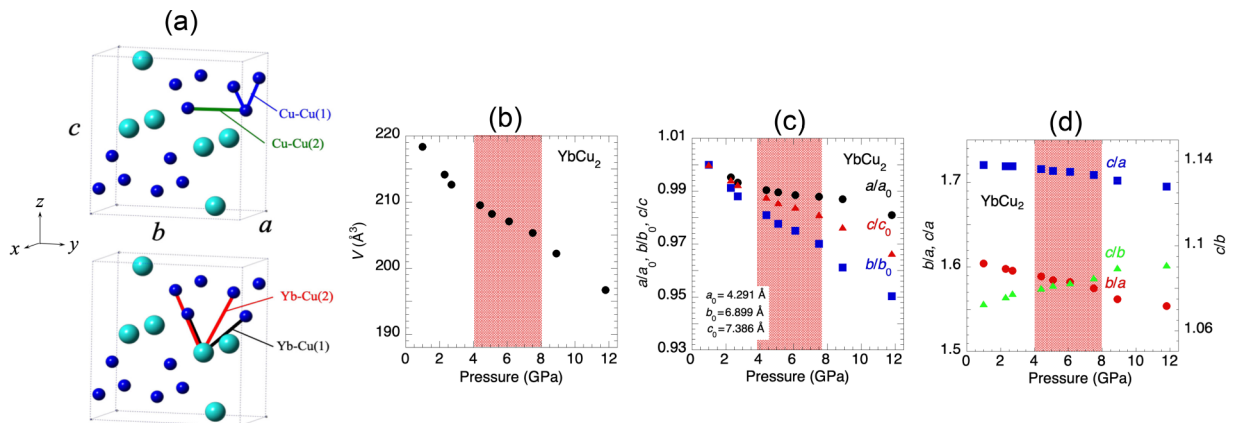


FIG. 4. (a) A schematic view of the YbCu₂ crystal structure. (b) Pressure dependence of the volume. A shaded area around 4–8 GPa corresponds to the pressure range of the valence transition in Fig. 1(f). (c) Pressure dependence of the normalized lattice parameters. (d) Pressure dependence of the ratios of the lattice constants. For the data where the error is not visible, the error is less than or equal to the symbol size.

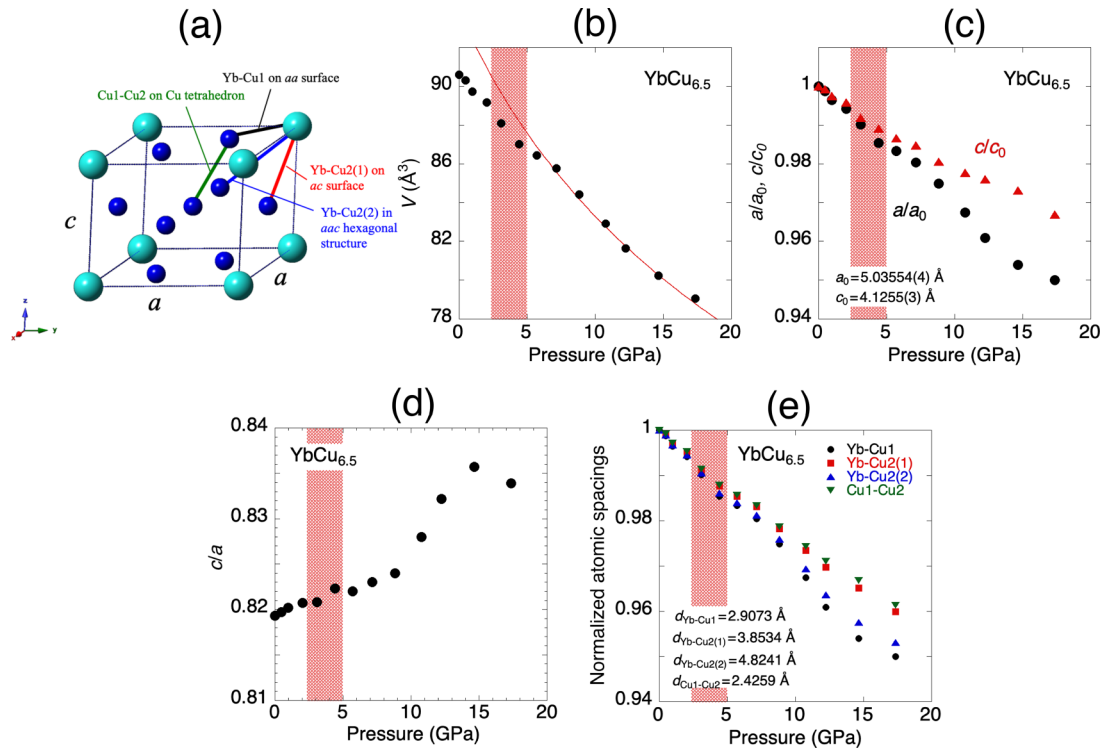


FIG. 5. (a) A schematic view of the $\text{YbCu}_{6.5}$ crystal structure. Here, it is noted that Ref. [13] suggested that 18% of the Yb site was randomly occupied by Cu-Cu dimers (not shown in the figure). (b) Pressure dependence of the volume. A shaded area corresponds to the pressure range of the valence transition in Fig. 1(f). (c) Pressure dependence of the normalized lattice parameters. (d) Pressure dependence of the ratio c/a of the lattice constants. (e) Pressure dependence of the normalized atomic spacing, where each distance is defined as shown in panel (a). For the data where the error is not visible, the error is less than or equal to the symbol size.

and the atomic spacings in $\text{YbCu}_{6.5}$, respectively. We fitted the XRD patterns of $\text{YbCu}_{6.5}$ with the $P6/mmm$ structure in all pressure ranges. The XRD patterns of $\text{YbCu}_{6.5}$ slightly changed above 12.2 GPa. This may be due to the nonhydrostatic condition by solidification of the pressure-transmitting medium which resulted in the peaks being broader. The crystal structure seems not to show a significant change around 3–4 GPa where the anomalous valence transition was observed. The c/a ratio of the lattice constants in Fig. 5(d) is a gradual change up to around 10 GPa, but it rises sharply at higher pressures above 10 GPa. This corresponds to a larger compressibility along the a axis compared to that along the c axis. Atomic distances also show similar changes to the volume and lattice constants as shown in Fig. 5(e).

The crystal of $\text{YbCu}_{6.5}$ is characteristic concerning the Yb-Cu distances. There are two kinds of Cu sites, Cu1 and Cu2, and the distance of Yb-Cu1 is much smaller than those of Yb-Cu2(1) and Yb-Cu2(2). Therefore, the hybridization between Yb and Cu may have a strong Cu site dependence in $\text{YbCu}_{6.5}$. The trend of the distances between Yb-Cu2(2) and Yb-Cu1 to decrease with pressure is different from that between Yb-Cu2(1) and Cu1-Cu2 as shown in Fig. 5(e). The former distances, Yb-Cu1 and Yb-Cu2(2), are on the aa surface and in the aac -hexagonal structure, respectively, as shown in Fig. 5(a). The latter distances, Yb-Cu2(1) and Cu1-Cu2, are on the ac surface and the Cu tetrahedron, respectively. The distances of Yb-Cu1 and Yb-Cu2(2) start to decrease more rapidly above around 10 GPa. Pressure dependences of the lattice constants of a in Fig. 5(c) also show

a more rapid decrease above 10 GPa compared to that of c . These pressure-induced changes in the distances of Yb-Cu1 and Yb-Cu2(2) reflect that in the lattice constant a . These changes seem to be correlated to those in the Yb valence above 10 GPa. Thus, the pressure-induced change in the Yb-Cu distances could be the origin of the increase of the Yb valence above 10 GPa in $\text{YbCu}_{6.5}$.

No structural phase transition was observed in $\text{YbCu}_{6.5}$ up to 17.4 GPa, including the pressure range around 3–4 GPa. The valence gradually increases with pressure above 10 GPa, and this normal change corresponds to the rapid increase of the ratio of the lattice in Fig. 5(d). On the other hand, pressure-induced change in the valence up to 10 GPa without structural phase transition is anomalous. We could consider the following scenario. Pressure-induced changes in the volume and lattice constant along the a axis become sharp above 7 GPa as shown in Figs. 5(b) and 5(c). Since the ionic radius of Yb^{3+} is smaller than that of Yb^{2+} , the transition to the Yb^{3+} state above 7 GPa is normal. In contrast, the change in the ratio of the lattice constants is gradual up to 10 GPa as shown in Fig. 5(d). The pressure dependence of the volume seems to be also gradual in the pressure range of 4–7 GPa, which may correspond to decompression as discussed in Ref. [11]; when we consider the volume change above 7 GPa is a normal compression, consequently, this possibly causes a decrease in the valence in this pressure range. However, the more direct reason for this anomalous valence transition is likely to be derived from the electronic structure of Cu above the Fermi level, the coexistence of two kinds of charge states

of Cu, which are described below. In $\text{YbCu}_{6.5}$, it is also likely to occur that the atomic distance between the Cu-Cu dimer site which replaces the 18% of the Yb site has changed by pressure [13], leading to the charge transfer from the Cu-Cu dimer to the Yb site. Unfortunately, the present resolution of the XRD patterns under pressure did not allow us to refine the atomic position of the Cu-Cu dimer site.

In Figs. 3(b), 3(f), and 5(b) we show fits of the pressure-volume relation by using an empirical formula of the Murnaghan equation of state [57], $\frac{V}{V_0} = [1 + p \frac{B'}{B_0}]^{-\frac{1}{B'}}$, where p , V , V_0 , B_0 , and B' are pressure, volume, volume at ambient pressure, bulk modulus of incompressibility, and fit first derivative with respect to the pressure, respectively. In Fig. 5(b) we fitted for the data above 8.8 GPa far above the valence transition pressure. We obtain the parameters of $B_0 = 62.0$ GPa, $B' = -0.301$, $V_0 = 187.0 \text{ \AA}^3$ for YbCu at the low-pressure phase; $B_0 = 101.2$ GPa, $B' = 1.65$, $V_0 = 40.3 \text{ \AA}^3$ for YbCu at the high-pressure phase; and $B_0 = 60.0$ GPa, $B' = 5.34$, $V_0 = 93.9 \text{ \AA}^3$ for $\text{YbCu}_{6.5}$. A small negative value of B' in YbCu is due to the nearly linear pressure dependence of the volume.

The temperature-induced first-order valence transition of YbInCu_4 had been believed not to accompany the structural transition [49,58]. However, later, it was found that the splitting of Bragg peaks at the 2θ angle greater than 90° was detected in high-order reflections below the Yb valence transition temperature in a single-crystal XRD experiment, indicating a structural change from a $F\bar{4}3m$ -cubic to a $\bar{4}m2$ -tetragonal structure [56]. The present measurements for the YbCu_x systems were performed for the powder samples and thus precise measurements of the XRD patterns for the single crystals under pressure have a potential to show a change in the crystal structure. This remains a challenge to study in the future.

C. XAS at the Cu L absorption edge

Complementary to the measurements of the electronic structure of the Yb site, we measured the high-resolution XAS spectra of the Cu site at the Cu- L_3 absorption edge for YbCu, YbCu_2 , $\text{YbCu}_{4.5}$, $\text{YbCu}_{6.5}$, and YbInCu_4 at 10 K with that for Cu_2O at 300 K as shown in Fig. 6(a). Both spectra of YbCu and YbCu_2 are similar to each other. The spectrum of Cu_2O reproduced well the previous results [59]. The single peak around 933 eV in Cu_2O was assigned to a $2p^5 3d^{10}$ final state coming from a $2p^6 3d^9$ initial state [60]. The spectra of YbCu_x are very different from the spectrum of Cu_2O , where Cu atoms are covalently bonded to the O atoms [59,61,62], but are similar to that of Cu metal [59] except $\text{YbCu}_{6.5}$. Theoretical calculations for fcc and bcc Cu metal suggested that the peak $P2$ at 935 eV and the peak $P3$ at 939 eV correspond to the transitions of $2p-3d$ and $2p-4s$, respectively [61]. The energy of the absorption edge shifts to higher energy at the order of $\text{YbCu} < \text{YbCu}_2 < \text{YbCu}_{4.5}$.

In YbInCu_4 a slight shift of the peak $P2$ to higher energy was observed with increasing the intensity of the peak $P1$ below the temperature of the valence transition, where the weak shoulder peak $P1$ was considered to be derived from the Cu $3d$ states [63]. It was suggested that the electron transfer from the Cu $3d$ sites to the Yb $4f$ sites occurred across the valence

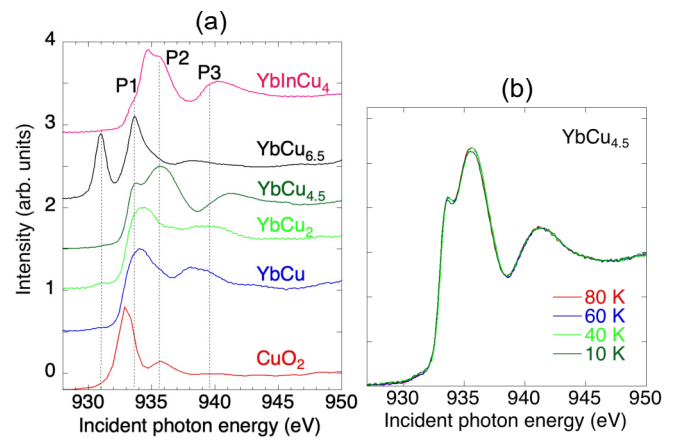


FIG. 6. (a) XAS spectra of YbCu, YbCu_2 , $\text{YbCu}_{4.5}$, $\text{YbCu}_{6.5}$, and YbInCu_4 at 10 K with the spectrum of Cu_2O at 300 K. (b) Temperature dependence of the XAS spectra of $\text{YbCu}_{4.5}$.

transition at low temperatures, resulting in the increase of the DOS of the Yb^{2+} states near the Fermi level. The peak intensity of YbCu and YbCu_2 corresponding to the peak $P1$ of YbInCu_4 is relatively stronger than that of $\text{YbCu}_{4.5}$. This suggests that the unoccupied states of Cu $3d$ of the former compounds are larger than those of the latter. This explains why the Yb valences of YbCu and YbCu_2 are smaller than that of $\text{YbCu}_{4.5}$.

The electronic structure of Cu in $\text{YbCu}_{6.5}$ above the Fermi level is very different from others as shown in Fig. 6(a), and rather similar to that of K_2NaCuF_6 [64]. $\text{YbCu}_{6.5}$ has a sharp and strong peak at 931 eV, which was not observed in YbCu, YbCu_2 , and $\text{YbCu}_{4.5}$. Two peaks around 931 and 934 eV could be assigned to be Cu^{2+} and Cu^{3+} states [62,65]. In $\text{YbCu}_{6.5}$ the XAS spectrum in Fig. 6(a) is likely to be a sum of the three different electronic states of Cu because of the three kinds of the Cu sites ($2c$, $3g$, and dimer Cu atoms at vacant Yb sites) [13]. The peak at 931 eV observed only for $\text{YbCu}_{6.5}$ is possibly caused by the Cu dimer site or one of the Cu sites in Fig. 5(a). A weak shoulder peak on the right of the 934-eV peak in $\text{YbCu}_{6.5}$ is due to the multiplet effect.

The Yb valence drastically decreased with pressure at low pressures in both $\text{YbCu}_{4.5}$ and $\text{YbCu}_{6.5}$ compounds [9]. In $\text{YbCu}_{4.5}$ the rapid decrease of the valence was considered to be caused by the structural phase transition [9]. However, there is no structural phase transition in $\text{YbCu}_{6.5}$ and the electronic structure of the Cu site of $\text{YbCu}_{6.5}$ is different from that of $\text{YbCu}_{4.5}$. X-ray absorption occurs for the unoccupied states above the Fermi level and the Fermi level corresponds to approximately the absorption edge of the XAS spectrum in the metallic compounds. Thus, the results may suggest a lower Fermi level in $\text{YbCu}_{6.5}$ compared to other YbCu_x compounds and it may correspond to the valence transition at a very low pressure of 3–4 GPa. We could consider a possible scenario for the valence transition in $\text{YbCu}_{6.5}$. When pressure is applied, the $4f$ level of the Yb^{2+} component shifts to the upper $5d$ band, and the charge transfer from the Yb $4f$ band to the $5d$ band occurs, resulting in the increase in the Yb valence normally [26,66,67]. However, the present results suggest that the inverse charge transfer from the Cu^{2+} to the

Yb^{3+} bands with pressure possibly occurs. A similar charge transfer from Cu to Yb was reported in YbInCu_4 , where the first-order valence transition was induced by decreasing the temperature and the Yb valence decreased toward the divalent state [63]. It is noted that Fig. 5 shows the lattice constants and the Yb-Cu and Cu-Cu distances decrease with pressure without a modification and the c/a ratio does not show a significant pressure dependence around the pressure range of the valence transition. Therefore, this valence transition may not be caused by the anomaly in the crystal structure. In $\text{YbCu}_{6.5}$ the existence of the Cu^{2+} state, the three kinds of Cu sites, and the electronic structure may play an important role in the anomalous valence transition. A theoretical study is desired to understand the exact mechanism of the anomalous valence transition in $\text{YbCu}_{6.5}$. Figure 6(b) shows the temperature dependence of the XAS spectra of $\text{YbCu}_{4.5}$ below 80 K. No temperature dependence was observed. In $\text{YbCu}_{4.5}$ the Yb valence decreased with decreasing the temperature from 2.94 at 100 K to 2.92 at 16 K [9]. The result in Fig. 6(b) indicates that the temperature-induced change in the electronic structure of the Cu sites is too small to observe in the present resolution.

IV. CONCLUSION

The electronic and crystal structures of YbCu , YbCu_2 , and $\text{YbCu}_{6.5}$ under pressure were measured by high-resolution x-ray absorption spectroscopy and x-ray diffraction. A first-order valence transition was found at 4 GPa in YbCu where no structural phase transition was observed. In YbCu the structural transition from the FeB-type to CsCl-type crystal structure around 10 GPa was found, whereas the Yb valence does not show a significant increase between 10 and 15 GPa, and it seems to show a small steplike increase of the valence at 15 GPa. Anomalies in pressure-induced valence changes in these systems have been found to correspond to anomalies in the lattice constants and atomic distances in YbCu and

YbCu_2 . In $\text{YbCu}_{6.5}$ pressure-induced anomalous valence transition was observed at low pressure, also without the structural transition. The Yb valence decreased approximately from 2.41 at 2.2 GPa to 2.1 at 5.1 GPa and increased gradually with further increase of the pressure. No anomaly in the crystal structure was observed in this pressure range.

The electronic structures of the Cu site of YbCu_x were also measured at the Cu- L_3 absorption edge at ambient pressure by x-ray absorption spectroscopy. The XAS spectra of YbCu and YbCu_2 are similar, but the spectrum of $\text{YbCu}_{6.5}$ was very different from others. In $\text{YbCu}_{6.5}$ a possibility of a charge transfer from Cu d to Yb $4f$ bands was discussed as an origin of the anomalous decrease in the Yb valence in $\text{YbCu}_{6.5}$ at low pressures. It was shown that the Cu-site-dependent decrease of the atomic distances could be an origin of the increase of the Yb valence above 10 GPa. We also measured the valence band spectra of YbCu_x , supporting the results of the PFY-XAS spectra for the Yb valence.

In YbCu_x , the crystal structure changed when the Cu composition was changed. We observed large pressure-induced valence changes despite the absence of a crystalline phase transition. However, commonly anomalous changes in the Yb valences were linked to anomalies in crystal structures.

ACKNOWLEDGMENTS

The experiments were performed at Taiwan beamlines BL12XU and BL12B2 at SPring-8 under Proposals No. 2017B4260, No. 2017B4267, No. 2018A4258, and No. 2018A4141 (corresponding Proposals No. 2017-2-179, No. 2018-1-039, No. 2018-1-012, and No. 2018-2-267 of NSRRC) and also beamlines BL-7 and BL-14 at HiSOR under Proposals No. 17AG009 and No. 18AG003. We thank the N-BARD, Hiroshima University for supplying the liquid helium. This work is supported by Grants in Aid for Scientific Research from the Japan Society for the Promotion of Science (Kiban Houga Grant No. 18K18743).

-
- [1] K. H. J. Buschow, Intermetallic compounds of rare earths and non-magnetic metals, *Rep. Prog. Phys.* **42**, 1373 (1979).
 - [2] J. M. Lawrence, P. S. Riseborough, and R. D. Parks, Valence fluctuation phenomena, *Rep. Prog. Phys.* **44**, 1 (1981).
 - [3] P. Strang, A. Svane, W. M. Temmerman, Z. Szotek, and H. Winter, Understanding the valency of rare earths from first-principles theory, *Nature (London)* **399**, 756 (1999).
 - [4] K. Kummer, C. Geibel, C. Krellner, G. Zwirgagl, C. Laubschat, N. B. Brookes, and D. V. Vyalikh, Similar temperature scale for valence changes in Kondo lattices with different Kondo temperatures, *Nat. Commun.* **9**, 2011 (2018).
 - [5] H. v. Löhneysen, A. Rosch, M. Vojta, and P. Wölfle, Fermi-liquid instabilities at magnetic quantum phase transitions, *Rev. Mod. Phys.* **79**, 1015 (2007).
 - [6] N. E. Bickers, D. L. Cox, and J. W. Wilkins, Self-consistent large- N expansion for normal-state properties of dilute magnetic alloys, *Phys. Rev. B* **36**, 2036 (1987).
 - [7] S. Doniach, The Kondo lattice and weak antiferromagnetism, *Physica B+C* **91**, 231 (1977).
 - [8] J. F. Herbst and J. W. Wilkins, Pressure-induced $4f$ occupancy enhancement in the rare-earth metals, *Phys. Rev. B* **29**, 5992 (1984).
 - [9] H. Yamaoka, N. Tsujii, Y. Yamamoto, Y. Michiue, J.-F. Lin, N. Hiraoka, H. Ishii, K.-D. Tsuei, and J. Mizuki, Reentrant valence transition in $\text{YbCu}_{4.5}$ under pressure, *Phys. Rev. B* **97**, 085106 (2018).
 - [10] H. Yamaoka, N. Tsujii, M.-T. Suzuki, Y. Yamamoto, I. Jarrige, H. Sato, J.-F. Lin, T. Mito, J. Mizuki, H. Sakurai, O. Sakai, N. Hiraoka, H. Ishii, K.-D. Tsuei, M. Giovannini, and E. Bauer, Pressure-induced anomalous valence crossover in cubic YbCu_5 -based compounds, *Sci. Rep.* **7**, 5846 (2017).
 - [11] H. Yamaoka, A. Ohmura, N. Tsujii, Y. Furue, H. Ishii, and N. Hiraoka, Electronic and crystal structures of YbInCu_4 -based compounds under pressure, *J. Phys. Soc. Jpn.* **92**, 064704 (2023).
 - [12] A. Iandelli and A. Palenzona, The ytterbium-copper system, *J. Less-Common Met.* **25**, 333 (1971).
 - [13] J. Hornstra and K. H. J. Buschow, The crystal structure of $\text{YbCu}_{6.5}$, *J. Less-Common Met.* **27**, 123 (1972).

- [14] M. Giovannini, R. Pasero, S. De Negri, and A. Saccone, Yb(Cu, T)₅ and Yb(Cu, T)_{4.5} solid solutions (T = Ag, Au, Pd), *Intermetallics* **16**, 399 (2008).
- [15] L. Spendeler, D. Jaccard, J. Sierro, M. François, A. Stepanov, and J. Voiron, Resistivity and thermoelectric power of YbCu_{4.5} under very high pressure, *J. Low Temp. Phys.* **94**, 585 (1994).
- [16] N. Tsujii, J. He, F. Amita, K. Yoshimura, K. Kosuge, H. Michor, G. Hilscher, and T. Goto, Kondo-lattice formation in cubic-phase YbCu₅, *Phys. Rev. B* **56**, 8103 (1997).
- [17] D. Debray, B. F. Wortmann, and S. Methfessel, Anomalous magnetic susceptibility behavior of some Yb compounds: Thermally excited interconfiguration crossover, *Phys. Rev. B* **14**, 4009 (1976).
- [18] B. D. Belan, O. I. Bodak, R. Cerny, J. V. Pacheco, and K. Yvon, Crystal structure of ytterbium copper, YbCu, *Z. Krist.: New Cryst. Struct.* **212**, 508 (1997).
- [19] D. Jaccard, A. Junod, and J. Sierro, Electrical resistivity, thermopower and specific heat of the intermediate valence system YbCu_x, *Helv. Phys. Acta* **53**, 583 (1980).
- [20] R. Černý, M. François, K. Yvon, D. Jaccard, E. Walker, V. Petříček, I. Čisárová, H.-U. Nissenk, and R. Wessicken, A single-crystal x-ray and HRTEM study of the heavy-fermion compound YbCu_{4.5}, *J. Phys.: Condens. Matter* **8**, 4485 (1996).
- [21] A. Amato, R. A. Fisher, N. E. Phillips, D. Jaccard, and E. Walker, Magnetic field dependence of the specific heat of heavy-fermion YbCu_{4.5}, *Phys. B: Condens. Matter* **165-166**, 389 (1990).
- [22] K. Hämäläinen, D. P. Siddons, J. B. Hastings, and L. E. Berman, Elimination of the inner-shell lifetime broadening in x-ray-absorption spectroscopy, *Phys. Rev. Lett.* **67**, 2850 (1991).
- [23] K. Hämäläinen, C. C. Kao, J. B. Hasting, D. P. Siddons, L. E. Berman, V. Stojanoff, and S. P. Cramer, Spin-dependent x-ray absorption of MnO and MnF₂, *Phys. Rev. B* **46**, 14274 (1992).
- [24] H. Yamaoka, Pressure dependence of the electronic structure of 4f and 3d electron systems studied by x-ray emission spectroscopy, *High Press. Res.* **36**, 262 (2016).
- [25] J. M. Lawrence, P. S. Riseborough, C. H. Booth, J. L. Sarrao, J. D. Thompson, and R. Osborn, Slow crossover in YbXCu₄ (X = Ag, Cd, In, Mg, Tl, Zn) intermediate-valence compounds, *Phys. Rev. B* **63**, 054427 (2001).
- [26] See Supplemental Material at <http://link.aps.org/supplemental/10.1103/PhysRevB.109.155147> for f electron number dependence of the volume for the LnCu (Ln: lanthanoid) family and the fit examples to the XRD patterns, which also includes Refs. [9,18,20,30,47,51–55,67,68]. Details of a promotional model are also described.
- [27] S. Gottlieb-Schönmeyer, S. Brühne, F. Ritter, W. Assmus, S. Balanetsky, M. Feuerbacher, T. Weber, and W. Steuer, Crystal growth of copper-rich ytterbium compounds: The predicted giant unit cell structures YbCu_{4.4} and YbCu_{4.25}, *Intermetallics* **17**, 6 (2009).
- [28] P. Popčević, I. Smiljanić, N. Barišić, A. Smontara, J. Dolinšek, and S. Gottlieb-Schönmeyer, Transport properties of YbCu_{4.4} giant-unit-cell metallic compound, *Croat. Chem. Acta* **83**, 69 (2010).
- [29] D. Jaccard, F. Haenssler, and J. Sierro, Pressure dependence of electrical resistivity and thermopower: Valence transition in YbCu₂ and TmSe, *Helv. Phys. Acta* **53**, 590 (1980).
- [30] H. Yamaoka, I. Jarrige, N. Tsujii, N. Hiraoka, H. Ishii, and K.-D. Tsuei, Temperature dependence of the Yb valence in YbCu₅ and YbCu_{5-x}Al_x Kondo compounds studied by x-ray spectroscopy, *Phys. Rev. B* **80**, 035120 (2009).
- [31] N. Sato, H. Abe, M. Kontani, S. Yamagata, K. Adachi, and T. Komatsubara, Magnetic properties of heavy fermion compounds YbCu_{3.5} and YbCu_{4.5}, *Phys. B: Condens. Matter* **163**, 325 (1990).
- [32] J. C. P. Klasse, F. R. de Boer, and P. F. de Chatel, Systematics in intermetallic compounds containing intermediate-valent ytterbium, *Physica B+C* **106**, 178 (1981).
- [33] Z. Fisk, J. D. Thompson, and H. R. Ott, Heavy-electrons: New materials, *J. Magn. Magn. Mater.* **76-77**, 637 (1988).
- [34] C. Rossel, K. N. Yang, M. B. Maple, Z. Fisk, E. Zirngiebl, and J. D. Thompson, Strong electronic correlations in a new class of Yb-based compounds: YXCu₄ (X = Ag, Au, Pd), *Phys. Rev. B* **35**, 1914 (1987).
- [35] A. Amato, R. A. Fisher, N. E. Phillips, D. Jaccard, and E. Walker, Pressure dependence of the specific heat of heavy-fermion YbCu_{4.5}, *Phys. B: Condens. Matter* **165-166**, 425 (1990).
- [36] H. Yamaoka, I. Jarrige, N. Tsujii, J.-F. Lin, N. Hiraoka, H. Ishii, and K.-D. Tsuei, Temperature and pressure-induced valence transitions in YbNi₂Ge₂ and YbPd₂Si₂, *Phys. Rev. B* **82**, 035111 (2010).
- [37] H. K. Mao and P. M. Bell, High-pressure physics: The 1-megabar mark on the Ruby R₁ static pressure scale, *Science* **191**, 851 (1976).
- [38] K. Syassen, Ruby under pressure, *High Press. Res.* **28**, 75 (2008).
- [39] A. P. Hammersley, S. O. Svensson, M. Hanfland, A. N. Fitch, and D. Hausermann, Two-dimensional detector software: From real detector to idealised image or two-theta scan, *High Press. Res.* **14**, 235 (1996).
- [40] H. M. Rietveld, A profile refinement method for nuclear and magnetic structures, *J. Appl. Cryst.* **2**, 65 (1969).
- [41] A. Le Bail, H. Duroy, and J. L. Fourquet, Ab-initio structure determination of LiSbWO₆ by x-ray powder diffraction, *Mater. Res. Bull.* **23**, 447 (1998).
- [42] We used the JANA2006 program to analyze the crystal structures.
- [43] M. Sawada, K. Yaji, M. Nagira, A. Kimura, H. Namatame, and M. Taniguchi, Design concept and performance of the soft x-ray beamline HiSOR-BL14, *AIP Conf. Proc.* **879**, 551 (2007).
- [44] H. Yamaoka, N. Tsujii, K. Yamamoto, A. M. Vlaicu, H. Oohashi, H. Yoshikawa, T. Tochio, Y. Ito, A. Chainani, and S. Shin, Systematic study of bulk sensitive spectroscopy in the valence transition of YbInCu₄-based compounds, *Phys. Rev. B* **78**, 045127 (2008).
- [45] J. C. P. Klaasse, W. C. M. Mattens, F. R. de Boer, and P. F. de Chatel, Ambiguous magnetic behaviour of some Yb-compounds, *Physica B+C* **86-88**, 234 (1977).
- [46] D. Debray, Crystal chemistry of the CeCu₂-type structure, *J. Less-Common Met.* **30**, 237 (1973).
- [47] A. Fujimori, T. Shimizu, and H. Yasuoka, Photoemission study of valence fluctuation in YbCu₂, *Phys. Rev. B* **35**, 8945 (1987).
- [48] I. Felner and I. Nowik, First-order valence phase transition in cubic Yb_xIn_{1-x}Cu₂, *Phys. Rev. B* **33**, 617 (1986).
- [49] H. Sato, K. Shimada, M. Arita, K. Hiraoka, K. Kojima, Y. Takeda, K. Yoshikawa, M. Sawada, M. Nakatake, H. Namatame, M. Taniguchi, Y. Takata, E. Ikenaga, S. Shin, K. Kobayashi, K. Tamasaku, Y. Nishino, D. Miwa, M. Yabashi,

- and T. Ishikawa, Valence transition of YbInCu₄ observed in hard x-ray photoemission spectra, *Phys. Rev. Lett.* **93**, 246404 (2004).
- [50] G. N. Chesnut and Y. K. Vohra, Structural and electronic transitions in Ytterbium metal to 202 GPa, *Phys. Rev. Lett.* **82**, 1712 (1999).
- [51] G. A. Costa, E. A. Franceschi, and A. Tawansi, Phase equilibria in the EuCu system, *J. Less Common Metals* **106**, 175 (1985).
- [52] C. C. Chao, H. L. Luo, and P. Duwez, CsCl-type compounds in binary alloys of rare-earth metals with zinc and copper, *J. Appl. Phys.* **35**, 257 (1964).
- [53] V. F. Degtyareva, F. Porsch, S. S. Khasanov, V. Sh. Shekhtman, and W. B. Holzapfel, Effect of pressure on structural properties of intermetallic *LnM* lanthanide compounds, *J. Alloys & Compds.* **246**, 248 (1997).
- [54] R. Caputo, C. Oran, A. Tekin, and P. Villars, Equiatomic binary phases of copper-rare earth elements: An overview of monocuprides from first-principles calculations, *Chem. Phys. Chem.* **24**, e202200718 (2023).
- [55] H. Mizoguchi, J. Bang, T. Inoshita, T. Kamiya, and H. Hosono, On the origin of the negative thermal expansion behavior of YCu, *Inorg. Chem.* **58**, 11819 (2019).
- [56] S. Tsutsui, K. Sugimoto, R. Tsunoda, Y. Hirose, T. Mito, R. Settai, and M. Mizumaki, First-order structural change accompanied by Yb valence transition in YbInCu₄, *J. Phys. Soc. Jpn.* **85**, 063602 (2016).
- [57] F. D. Murnaghan, The compressibility of media under extreme pressures, *Proc. Natl. Acad. Sci. USA* **30**, 244 (1944).
- [58] Y. Utsumi, H. Sato, C. Moriyoshi, Y. Kuroiwa, H. Namatame, M. Taniguchi, K. Hiraoka, K. Kojima, and K. Sugimoto, Synchrotron radiation diffraction study of YbInCu₄, *Jpn. J. Appl. Phys.* **50**, 05FC10 (2011).
- [59] M. Finazzi, G. Ghiringhelli, O. Tjernberg, Ph. Ohresser, and N. B. Brookes, Radiationless Raman versus Auger behavior at the Cu *L*₃ resonance of CuO and Cu₂O, *Phys. Rev. B* **61**, 4629 (2000).
- [60] M.-J. Huang, G. Deng, Y. Y. Chin, Z. Hu, J.-G. Cheng, F. C. Chou, K. Conder, J.-S. Zhou, T.-W. Pi, J. B. Goodenough, H.-J. Lin, and C. T. Chen, Determination of hole distribution in Sr_{14-x}Ca_xCu₂₄O₄₁ using soft x-ray absorption spectroscopy at the Cu *L*₃ edge, *Phys. Rev. B* **88**, 014520 (2013).
- [61] H. Ebert, J. Stöhr, S. S. P. Parkin, M. Samant, and A. Nilsson, *L*-edge x-ray absorption in fcc and bcc Cu metal: Comparison of experimental and first-principles theoretical results, *Phys. Rev. B* **53**, 16067 (1996).
- [62] P. Jiang, D. Prendergast, F. Borondics, S. Porsgaard, L. Giovanetti, E. Pach, J. Newberg, H. Bluhm, F. Besenbacher, and M. Salmeron, Experimental and theoretical investigation of the electronic structure of Cu₂O and CuO thin films on Cu(110) using x-ray photoelectron and absorption spectroscopy, *J. Chem. Phys.* **138**, 024704 (2013).
- [63] Y. Utsumi, H. Sato, H. Kurihara, H. Maso, K. Hiraoka, K. Kojima, K. Tobimatsu, T. Ohkochi, S.-I. Fujimori, Y. Takeda, Y. Saitoh, K. Mimura, S. Ueda, Y. Yamashita, H. Yoshikawa, K. Kobayashi, T. Oguchi, K. Shimada, H. Namatame, and M. Taniguchi, Conduction-band electronic states of YbInCu₄ studied by photoemission and soft x-ray absorption spectroscopies, *Phys. Rev. B* **84**, 115143 (2011).
- [64] C. De Nadaï, A. Demourgues, J. Grannec, and F. M. F. de Groot, *L*_{2,3} x-ray absorption spectroscopy and multiplet calculations for KMF₃ and K₂NaMF₆ (*M* = Ni, Cu), *Phys. Rev. B* **63**, 125123 (2001).
- [65] J. Ghijsen, L. H. Tjeng, J. van Elp, H. Eskes, J. Westerink, G. A. Sawatzky, and M. T. Czyzyk, Electronic structure of Cu₂O and CuO, *Phys. Rev. B* **38**, 11322 (1988).
- [66] E. R. Ylvisaker, J. Kuneš, A. K. McMahan, and W. E. Pickett, Charge fluctuations and the valence transition in Yb under pressure, *Phys. Rev. Lett.* **102**, 246401 (2009).
- [67] I. Jarrige, H. Yamaoka, J.-P. Rueff, J.-F. Lin, M. Taguchi, N. Hiraoka, H. Ishii, K.-D. Tsuei, K. Imura, T. Matsumura, A. Ochiai, H. S. Suzuki, and A. Kotani, Unified understanding of the valence transition in the rare-earth monochalcogenides under pressure, *Phys. Rev. B* **87**, 115107 (2013).
- [68] H. Yamaoka, P. Thunström, N. Tsujii, I. Jarrige, K. Shimada, M. Arita, H. Iwasawa, H. Hayashi, J. Jiang, H. Namatame, M. Taniguchi, N. Hiraoka, H. Ishii, K.-D. Tsuei, M. Giovannini, and E. Bauer, The electronic structure and the valence state of Yb₂Pd₂Sn and YbPd₂Sn studied by photoelectron and resonant x-ray emission spectroscopies, *Phys. Rev. B* **86**, 085137 (2012).